Giant negative mobility of Janus particles in a corrugated channel

Pulak K. Ghosh,[1] Peter Hänggi,[2,3] Fabio Marchesoni,[4,5] and Franco Nori[5,6]

[1]*Department of Chemistry, Presidency University, Kolkata 700073, India*

[2]*Institut für Physik, Universität Augsburg, D-86135 Augsburg, Germany*

[3]*Center for Phononics and Thermal Energy Science and School of Physical Science and Engineering, Tongji University,
200092 Shanghai, People's Republic of China*

[4]*Dipartimento di Fisica, Università di Camerino, I-62032 Camerino, Italy*

[5]*CEMS, RIKEN, Saitama, 351-0198, Japan*

[6]*Physics Department, University of Michigan, Ann Arbor, Michigan 48109-1040, USA*

We numerically simulate the transport of elliptic Janus particles along narrow two-dimensional channels with reflecting walls. The self-propulsion velocity of the particle is oriented along either its major (prolate) or minor axis (oblate). In smooth channels, we observe long diffusion transients: ballistic for prolate particles and zero diffusion for oblate particles. Placed in a rough channel, prolate particles tend to drift against an applied drive by tumbling over the wall protrusions; for appropriate aspect ratios, the modulus of their negative mobility grows exceedingly large (giant negative mobility). This suggests that a small external drive suffices to efficiently direct self-propulsion of rod-like Janus particles in rough channels.

I. INTRODUCTION

Self-propulsion [1] is the ability of most living organisms to move, in the absence of external drives, thanks to an "engine" of their own. Self-propulsion of fabricated micro- and nanoparticles (artificial microswimmers) [2–5] is a topic of current interest in view of applications to nanotechnology. Their direct experimental observation became affordable with the synthesis of a new class of asymmetric microswimmers, which propel themselves by generating local gradients in the suspension environment (self-phoretic effects) [6]. Such particles, called Janus particles (JPs) [7,8], consist of two distinct sides, only one of which is chemically or physically active. Thanks to their functional asymmetry, these active particles can induce either concentration gradients (self-diffusiophoresis) by catalyzing a chemical reaction on their active surface [9–12], or thermal gradients (self-thermophoresis), e.g., by inhomogeneous light absorption [13] or magnetic excitation [14].

Much effort is presently directed toward achieving reliable transport control of JPs in confined geometries [15–17]. The ability of Janus microswimmers to perform directed autonomous motions through periodic arrays [12] and asymmetric channels [18] surely is a suggestive option. Such devices do operate in the absence of external drives or gradients, but at the price of strict fabrication requirements regarding their geometry. In this paper we propose a more affordable option to direct the motion of JPs along a channel. Under appropriate conditions involving the geometry of both the particle and the channel, a tiny external drive (even in the absence of other biases) can orient the self-propulsion velocity of the microswimmers *against* the drive, a phenomenon known as absolute negative mobility (ANM) [19]. The roughness of the channel walls, mimicked here by randomly inserting small transverse wall protrusions, can drastically enhance this phenomenon, thus producing a *giant* absolute negative mobility. These features suggest most sensitive control techniques on JP transport with beneficial applications to nanotechnology and medical sciences [2,7].

II. MODEL

Shape is known to play a central role in the diffusive dynamics of confined JPs [20,21]. For this reason we consider two-dimensional (2D) channels and elongated particles, modeled as elliptical disks with semiaxes a and b. Actual rod-like JPs can be synthesized through a variety of well-established techniques [15,20,22]. An elongated JP gets a continuous push from the suspension fluid, which in the overdamped regime amounts to a self-propulsion velocity $\mathbf{v}_0$ with constant modulus v_0. Additional dynamical effects, neglected in the present model, are briefly discussed at the end. We assume that $\mathbf{v}_0$ acts along the a axis of the particle: $\mathbf{v}_0$ is parallel to the particle major axis for $a > b$ (prolate JP) and orthogonal to it for $a < b$ (oblate JP). The self-propulsion direction varies randomly with time constant τ_θ; accordingly, the microswimmer mean self-propulsion path is $l_\theta = v_0 \tau_\theta$.

The bulk dynamics of such a JP obeys the Langevin equation [23]

$$\dot{\mathbf{r}} = \mathbf{v}_0(t) + \mathbf{F} + \xi_0(t), \qquad (1)$$

where $\mathbf{r} = (x,y)$ denotes the position of the particle center of mass, $\mathbf{F} = (F,0)$ represents a d.c. external bias parallel to the channel axis, and $\xi_0(t) = (\xi_{0,x}(t),\xi_{0,y}(t))$ models a Gaussian thermal noise with $\langle \xi_{0,i}(t) \rangle = 0$ and $\langle \xi_{0,i}(t)\xi_{0,j}(0) \rangle = 2D_0 \delta_{ij}\delta(t)$, with $i,j = x,y$, The self-propulsion velocity $\mathbf{v}_0 = v_0(\cos\theta, \sin\theta)$ is oriented at an angle $\theta(t)$ with respect to the x axis, where $\theta(t)$ is a Wiener process, $\dot{\theta} = \xi_\theta(t)$, with $\langle \xi_\theta(t) \rangle = 0$ and $\langle \xi_\theta(t)\xi_\theta(0) \rangle = 2D_\theta \delta(t)$. As a change in θ corresponds to a rotation of the swimmer, D_θ is related to both τ_θ, $D_\theta = 2/\tau_\theta$ [18,23], and the average thermal diffusivity D_0, $D_\theta \propto D_0/ab$ [24]. To make contact with realistic experimental conditions in our simulations we chose parameters experimentally accessible. For instance, expressing times in seconds and lengths in microns, typical values for spherical JP of radius 0.5–2.0 are $D_0 = 0.02$–0.03, $D_\theta = 0.01$, and $v_0 = 0.05$–0.5 [12].

When confined to a cavity of size smaller than its self-propulsion length l_θ, the microswimmer undergoes multiple collisions with the walls and the confining geometry comes into play (Knudsen diffusion [25]). The Langevin equations (1) have been numerically integrated under the assumption that the channel walls were perfectly reflecting and the particle-wall collisions elastic [26].

III. DIFFUSION TRANSIENTS

Transport of elongated JPs along a smooth channel is characterized by unit mobility, $\mu = 1$, where $\mu \equiv v/F$ and $v(F) = \lim_{t\to\infty}\langle x(t)\rangle/t$. The particle shape becomes distinguishable when one looks at the dispersion $\Delta x^2(t) = \langle x^2(t)\rangle - \langle x(t)\rangle^2$. Both prolate and oblate disks undergo surprisingly long transients, see Fig. 1, before the expected normal diffusion regime sets in. On the contrary, circular disks seem to diffuse like ordinary point-like JPs [18,23]: for $t \gtrsim \tau_\theta$, $\Delta x^2(t) = 2D_{\text{eff}}t$ with $D_{\text{eff}} = D_0 + v_0 l_\theta/4$. Due to their collision against the walls, active prolate swimmers tend to slide parallel to the channel axis, which explains their ballistic diffusion transient with $\Delta x^2(t) \sim (v_0 t)^2$, whereas oblate swimmers tend to pile up against the walls, thus suppressing longitudinal diffusion. Upon increasing the strength of the thermal noise D_0, both transients are shortened, though at a different rate. This property can be explained by noticing that the onset of normal diffusion requires that the microswimmers are capable of inverting the direction of $\mathbf{v}_0$ against the confining action of the channel walls. On the other hand, a ∪ turn can only occur when noise kicks the elongated particle out of its steady (sliding or stuck) state. This amounts to a noise-activated process with time constant of the order of [26] $\tau_U \simeq \tau_0 \exp(|a - b|v_0/D_0)$, where $\tau_0 \sim \sqrt{v_0 a^2/b}$. Accordingly, for the a and b values
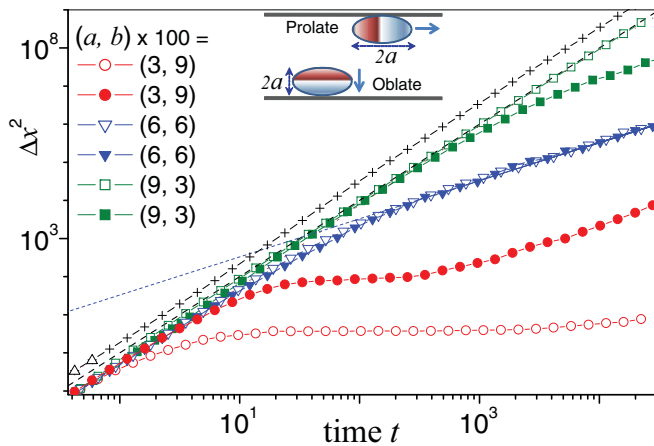
of Fig. 1, transients are longer for the prolate than for the oblate particle. When τ_U becomes of the order of or smaller than the crossing time y_L/v_0, boundary effects vanish and (bulk) normal diffusion is fully restored, i.e., transients become negligible. For strongly prolate, say, rod-like swimmers, ballistic transients may extend over exceedingly long time intervals even at room temperature (see example in Fig. 1). For this reason determining how dispersion scales with time can prove a delicate experimental issue [2].

IV. ABSOLUTE NEGATIVE MOBILITY

We consider now the case of a periodically compartmentalized channel obtained by inserting equally spaced transverse dividers, each bearing a small opening, or pore, centered on the channel axis. Let x_L and y_L be the longitudinal and transverse dimensions of the compartments and Δ the pore size (see sketch in Fig. 3). Such a channel is termed septate [27–29] to stress the role of the compartment walls when compared with the smooth cross-section modulation of the so-called entropic channels [30]. Here, transport of elongated swimmers is governed by the pore crossing dynamics, which makes the mobility shape dependent.

In Figs. 2 and 3 we plot the mobility of prolate JPs as a function of the drive for different values of the aspect ratio a/b and the orientation constant D_θ. The most prominent feature is the appearance of ANM branches at low F, which means that under certain conditions, active swimmers may drift against the applied drive [19]. This effect (i) grows more apparent for large aspect ratios, a/b (Fig. 2); (ii) is limited to the domain $F < v_0$; (iii) does not occur for oblate particles (an example was added to the inset of Fig. 2); and (iv) exhibits a resonant dependence
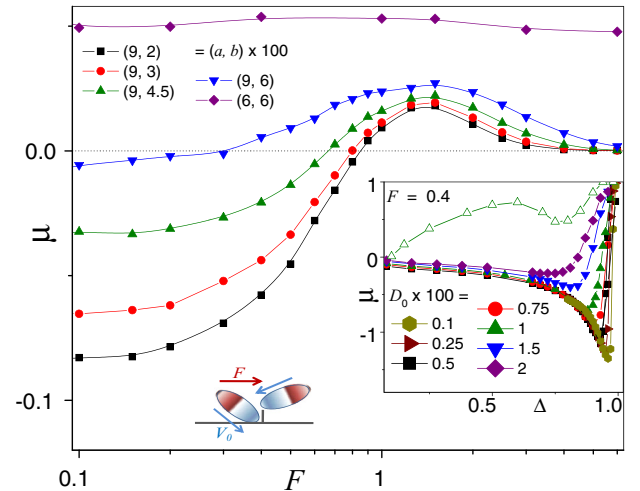

FIG. 1. (Color online) Diffusion of elliptical JPs with semiaxes a and b (see legend) in a smooth channel of width $y_L = 1$. Thermal noise is $D_0 = 10^{-4}$ (empty symbols) and 6.4×10^{-3} (filled symbols); self-propulsion parameters are $v_0 = 1$ and $D_\theta = 0.03$. The ballistic transient, $\Delta x^2 = (v_0 t)^2$ (dashed line), and the normal diffusion law, $\Delta x^2 = 2D_{\text{eff}}t$ (see text, dotted line) are drawn for a comparison. Example of persistent ballistic diffusion transient (crosses): $a = 0.15$, $b = 0.03$, $y_L = 10$, $v_0 = 2$, $D_0 = 0.02$, and $D_\theta = 0.003$ [12]. Sketch: sliding prolate (top) and stuck oblate (bottom) disks. In both cases, $\mathbf{v}_0$ (single-pointed arrow) is oriented along the a axis.

FIG. 2. (Color online) Mobility $\mu(F)$ of a prolate JP driven along a septate channel for different values of its semiaxes a and b (see legend). Compartment parameters: $x_L = y_L = 1$ and $\Delta = 0.16$; self-propulsion parameters: $v_0 = 1$ and $D_\theta = D_0 = 0.03$. Inset: μ vs Δ for $F = 0.4$, $a = 0.09$, $b = 0.03$, and different D_0 (solid symbols). The curve (empty triangles) for the oblate JP with $a = 0.03$, $b = 0.09$ at $D_0 = 0.01$ is plotted for comparison. All the remaining parameters are as in the main panel. Sketch: a prolate JP tumbling over a winglet of the channel wall under the action of the drive (see text).
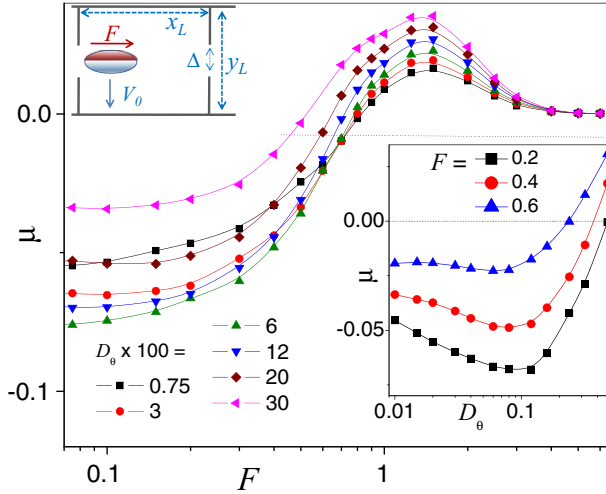
FIG. 3. (Color online) Mobility $\mu(F)$ of a prolate JP driven along a septate channel for different values of D_θ (i.e., the reciprocal of τ_θ, see legend). Compartment parameters: $x_L = y_L = 1$ and $\Delta = 0.16$; other simulation parameters: $v_0 = 1$, $a = 0.09$, $b = 0.03$, and $D_0 = 0.03$. Inset: μ vs D_θ for different F. All remaining parameters are as in the main panel. Sketch: oblate JP aligned so as to leave a septate compartment to the left, being pulled back by F.

on $\tau_\theta = 2/D_\theta$ (Fig. 3, inset). For larger F the mobility turns positive, reaches a maximum, and finally decays to zero faster than $1/F$ (*negative differential mobility* branch).

We now qualitatively interpret these properties by having recourse to the analytical arguments of Refs. [29]. First of all, the ANM mechanism can be explained by recalling that a driven prolate particle gets pressed longitudinally against the side walls of the channel compartments. As in Figs. 2 and 3, $\Delta < 2a$, the particle can slip through the wall openings only by rotating with $\mathbf{v}_0$ (almost) orthogonal to the channel cross section [26]. Again, this is a noise-activated mechanism with Arrhenius factor $\exp[-|a - b|(F \pm v_0)/D_0]$, the sign $\pm$ denoting the parallel or antiparallel orientation of $\mathbf{v}_0$ with respect to $\mathbf{F}$. Therefore, pore crossings are more likely to take place on the left side of the compartment than on its right side; hence the observed negative mobility. This argument also leads to the conclusion that ANM is ruled out for prolate JPs with $F \gtrsim v_0$ and oblate JPs at any drive. This standstill at zero current crossing with $\mu(F) = 0$ for prolate microswimmers shifts to lower F on increasing D_0, because dispersion induced by thermal fluctuations tends to hamper the particle drift opposite to the drive. An oblate microswimmer, oriented with its major axis orthogonal to the compartment wall tends to propel itself parallel to (rather than against) it, whereas the drive pulls it back to the right (see sketch in Fig. 3). This state of affairs cannot be overturned by thermal noise. Thus, for an oblate JP, pore crossings to the right are favored and the mobility is always positive.

For large drives, $F \gg v_0$, the particle mobility is suppressed. This is a typical effect characteristic of septate channels [28], which is not observed in smoothly corrugated channels [30]. The particle leaves the compartment to the right, thus advancing a length x_L; however, after an activation time $\tau_\perp \propto \exp[|a - b|(F + v_0)/D_0]$, it needs to line up with

the pore axis. Accordingly, $\mu \sim x_L/(2\tau_\perp F)$, in fairly good agreement with our data. Finally, the inset of Fig. 3 clearly indicates that the ANM is maximal for an optimal choice of $\tau_\theta = 2/D_\theta$ (or l_θ). Note that for $\tau_\theta \to 0$, the active random motion of a JP becomes a standard Brownian motion with Einstein bulk diffusivity D_{eff}, and therefore its mobility must be positive. On the other hand, an elongated particle slips through a pore when, after turning perpendicular to the compartment wall, it diffuses toward the pore in a time $\tau_\parallel \sim y_l^2/2D_0$, which is no longer than its orientation time constant τ_θ. Based on our data, an optimal ANM at constant F, with $F < v_0$, is thus achieved by setting $\tau_\parallel \sim \tau_\theta$.

We mention in passing that we detected ANM also by driving prolate JPs along sinusoidally corrugated channels (not shown). Contrary to what happens in septate channels, negative mobility sets in for more elongated particles, i.e., at higher a/b, and μ approaches unity in the limit of large drives, $F \gg v_0$.

V. GIANT ABSOLUTE NEGATIVE MOBILITY

The magnitude of the backward rectification flow also depends on the compartment geometry and, in particular, on the pore size Δ. In the inset of Fig. 2 we plotted the mobility of a prolate JP versus Δ for $F < v_0$ and different noise levels D_0. The modulus of the negative mobility $|\mu|$ grows with Δ up to an optimal value Δ_M, which decreases with raising D_0; for $\Delta > \Delta_M$ the mobility jumps abruptly to its bulk value, $\mu = 1$. This behavior is surprising because the ANM mechanism relies on the blocking action of the compartment walls [19]. In the case of an elongated particle such an action is strongest when $\mathbf{F}$ and $\mathbf{v}_0$ point in the same direction [26], which causes a rectification flow against $\mathbf{F}$, i.e., negative mobility. However, as the pore size grows larger than the particle length, $\Delta \gtrsim 2a$, one would expect ANM to vanish. *Our data prove exactly the opposite*. More remarkably, on increasing Δ, $|\mu|$ overshoots to its maximum value consistent with the ANM mechanism, that is, $|\mu_M^{\text{ANM}}| = (v_0 - F)/(2F)$. This estimate of $|\mu_M^{\text{ANM}}|$ refers to the ideal optimistic case when a noiseless driven particle exits unhindered the channel compartments to the left with speed $v_0 - F$ for half of the time, whereas during the rest of the time it sits stuck against the right compartment walls. Note that spontaneous-direction reversals occur on the time scale τ_θ. Most remarkably, the low-noise curves $\mu(\Delta)$ in the inset of Fig. 2 exhibit sharp minima with $|\mu_M = \mu(\Delta_M)|$ about twice the ANM estimate $|\mu_M^{\text{ANM}}|$.

A simple explanation of this finding is illustrated by the sketch inserted also in Fig. 2. The large values of $|\mu_M|$ we observed imply that the *self-propulsion velocity of the driven JP (almost) always points against* $\mathbf{F}$. For a particle confined to a narrow channel with $l_\theta \gg y_L$, this is certainly true for half the time. For the remaining half of the time, however, $\mathbf{v}_0$ would spontaneously orient itself parallel to $\mathbf{F}$. This means that the collisions with the walls [and not the fluctuations of $\theta(t)$] must be responsible for the quick rotation of $\mathbf{v}_0$ to the opposite direction. For large Δ the compartment walls shrink to a pair of perpendicular winglets of length $\delta = (y_L - \Delta)/2$, sticking out of the channel walls. An elongated microswimmer hitting one such obstacle from the left, tumbles over it under the action of the torque exerted by the drive.
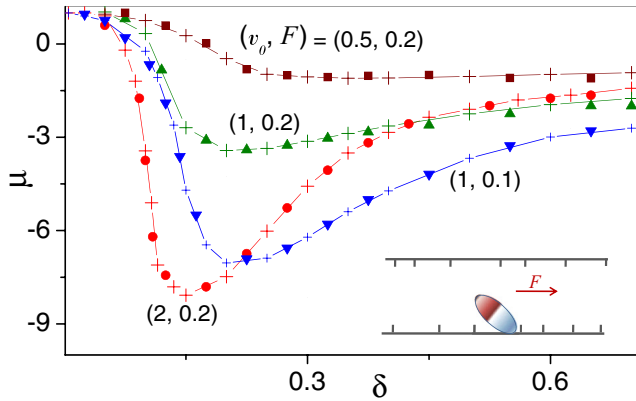
FIG. 4. (Color online) Giant negative mobility for a prolate JP driven along a rough channel of width $y_L = 10$ with different v_0 and F (see legend). On both sides winglets of length δ are separated by a random distance l_n, uniformly distributed in the interval [5,15] (solid symbols, see text); for a comparison we also simulated the corresponding case of equally spaced winglets with $l_n = 10$ (crosses). Other simulation parameters are $a = 1$, $b = 0.25$, $D_0 = 0.02$, and $D_\theta = 6 \times 10^{-3}$.

Of course, such a tumbling mechanism is most effective under a few simple conditions: (i) the tumbling time, $\tau_\delta \sim \pi I/Fa$, with $I = (a^2 + b^2)/4$ denoting the moment of inertia of an elliptical disk of unit mass, has to be much shorter than τ_θ; (ii) δ has to be the shortest possible, to minimize the blocking action of the compartment walls; (iii) the noise level has to be lowered as much as possible, lest the particle diffuses past the obstacle without tumbling. An optimal choice for δ seems $\delta_M \sim b/2$, which corresponds to $\Delta_M \sim y_L - b$ (see Fig. 2, inset). For shorter δ the particle can slide over the obstacle without rotating. Under these conditions $\mu_M \simeq -(v_0 - F)/F$ and its modulus can grow very large, indeed! We propose to call this phenomenon *giant negative mobility* (GNM).

GNM is sustained by the self-propulsion of the driven microswimmers themselves, the drive just helping to orient their velocities opposite to it. In such a scheme, contrary to ANM [19], the obstacles fabricated along the channel walls do not act as traps, but rather as centers of rotation (tumbling). To better assess the robustness of GNM, in Fig. 4 we plotted μ versus δ for both periodically and randomly distributed winglets, all of the same length δ. Randomized winglet distributions have been generated by scrambling regular distributions with period x_L, that is, by spacing the winglets a distance l_n apart, with $l_n = x_{n+1} - x_n = x_L(1 + \delta_n)$, x_n being the position of the nth winglet and δ_n a random number uniformly distributed in the interval [−0.5,0.5]. To more closely mimic wall roughness, the winglet distributions on the upper and lower channel walls were independently generated. We selected particle and compartment sizes consistent with the experimental setups described in the literature [12]. For both winglet distributions our estimates for Δ_M and μ_M work quite well, meaning that GNM ought to be experimentally detectable at room temperature.

For all curves displayed in Fig. 4, $|\mu_M|$ comes quite close to its upper bound $2|\mu_M^{\text{ANM}}|$. As anticipated, on lowering the self-propulsion diffusivity, $v_0^2/2D_\theta$, against D_0, the optimal

winglet length δ_M shifts to higher values and $|\mu_M|$ slowly diminishes. Moreover, since particle tumbling is a local mechanism, GNM is rather insensitive to the actual distribution of the channel winglets. Analogously, winglets can be replaced by protrusions of different geometry to better model the roughness of channel walls. As long as they are sharp enough to engage the tips of rod-like JPs, the GNM mechanism does work (possibly facilitated by the hydrodynamic attraction between microswimmers and channel walls); if not, the smooth channel situation discussed at the very beginning would be recovered.

To emphasize the mechanisms responsible for the negative mobility of elongated JPs, in Eq. (1) we neglected a number of additional effects which may prove experimentally appreciable. We started assuming that self-propulsion is fully described by the random velocity $\mathbf{v}_0$, thus implying the absence of chiral (or torque) and inertial (or viscous) terms [31]. We also adopted scalar translational diffusivity D_0 and orientational diffusivity D_c, despite the elongated shape of the active swimmer. A more detailed modeling of the active rototranslational dynamics [24] would have no substantial impact on the occurrence of negative mobility; the corresponding hydrodynamic corrections to the particle dynamics can be accounted for by an appropriate rescaling of the model parameters [32]. More important, we ignored hydrodynamic effects, which not only favor clustering in dense mixtures of JPs [33,34], but also may even cause their capture by the channel walls [35]. Therefore, in the case of single diffusing JPs, hydrodynamic effects can only reinforce the flow of particles at the boundary, thus enhancing the predicted diffusion transients and the tumbling mechanism responsible for GNM. On the contrary, hydrodynamic effects are known to impact on the selective translocation of elongated JPs through narrow pores [36], $\Delta \gg y_L$, and therefore are likely to hamper the direct observation of ANM.

VI. CONCLUSIONS

We numerically simulated the transport of elongated Janus particles driven along a narrow channel. Key transport quantifiers, like mobility and diffusivity, strongly depend on the particle shape. Diffusion in smooth channels is characterized by exceedingly long transients, either ballistic or nondiffusive, respectively, for prolate and oblate active microswimmers. In compartmentalized channels with narrow pores, prolate Janus particles undergo absolute negative mobility, as an effect of the translational symmetry breaking due to the drive. More important, when the compartment dividers shrink to small side winglets, possibly randomly distributed along the channel walls, rod-like active particles greatly enhance their negative mobility, as the combined action of drive and channel roughness systematically reorients the particle self-propulsion velocity opposite to the drive itself. Since the geometric and dynamical parameters used in our simulations closely compare with those reported for actual experimental setups, we are confident that giant negative mobility can soon be demonstrated, thus allowing a more effective transport control of active microswimmers. Such a control technique can be exploited, e.g., for medical applications, such as drug delivery via JPs to opposing physiological regions. Moreover, a dilute binary mixture of JPs of different shape can be driven along one such stylized rough channel so as to generate two-way traffic

(i.e., with mobilities of opposite sign) without having recourse to a parallel two-channel architecture with opposite drives.

ACKNOWLEDGMENTS

[1] E. M. Purcell, Am. J. Phys. **45**, 3 (1977).

[2] F. Schweitzer, *Brownian Agents and Active Particles* (Springer, Berlin, 2003).

[3] S. Ramaswamy, Annu. Rev. Condens. Matter Phys. **1**, 323 (2010).

[4] P. Romanczuk, M. Bär, W. Ebeling, B. Lindner, and L. Schimansky-Geier, Eur. Phys. J. Special Topics **202**, 1 (2012).

[5] T. Vicsek and A. Zafeiris, Phys. Rep. **517**, 71 (2012).

[6] see, e.g., Y. Hong, D. Velegol, N. Chaturvedi, and A. Sen, Phys. Chem. Chem. Phys. **12**, 1423 (2010).

[7] S. Jiang and S. Granick (eds.), *Janus Particle Synthesis, Self-Assembly and Applications* (RSC, Cambridge, England, 2012).

[8] A. Walther and A. H. E. Müller, Chem. Rev. **113**, 5194 (2013).

[9] W. F. Paxton, S. Sundararajan, T. E. Mallouk, and A. Sen, Angew. Chem. Int. Ed. **45**, 5420 (2006).

[10] J. G. Gibbs and Y.-P. Zhao, Appl. Phys. Lett. **94**, 163104 (2009).

[11] J. R. Howse, R. A. L. Jones, A. J. Ryan, T. Gough, R. Vafabakhsh, and R. Golestanian, Phys. Rev. Lett. **99**, 048102 (2007).

[12] G. Volpe, I. Buttinoni, D. Vogt, H.-J. Kümmerer, and C. Bechinger, Soft Matter **7**, 8810 (2011).

[13] H. R. Jiang, N. Yoshinaga, and M. Sano, Phys. Rev. Lett. **105**, 268302 (2010).

[14] L. Baraban, R. Streubel, D. Makarov, L. Han, D. Karnaushenko, O. G. Schmidt, and G. Cuniberti, ACS Nano **7**, 1360 (2013).

[15] S. Sengupta, M. E. Ibele, and A. Sen, Angew. Chem. Int. Ed. **51**, 8434 (2012).

[16] P. Hänggi and F. Marchesoni, Rev. Mod. Phys. **81**, 387 (2009).

[17] P. Hänggi, F. Marchesoni, and F. Nori, Ann. Phys. (Berlin) **14**, 51 (2005).

[18] P. K. Ghosh, V. R. Misko, F. Marchesoni, and F. Nori, Phys. Rev. Lett. **110**, 268301 (2013).

[19] R. Eichhorn, P. Reimann, and P. Hänggi, Phys. Rev. Lett. **88**, 190601 (2002); Phys. Rev. E **66**, 066132 (2002).

[20] F. Lugli, E. Brini, and F. Zerbetto, J. Chem. Phys. C **116**, 592 (2012).

[21] H. Noguchi and G. Gompper, Proc. Natl. Acad. Sci. U.S.A. **102**, 14159 (2005).

[22] Y. Hong, N. M. K. Blackman, N. D. Kopp, A. Sen, and D. Velegol, Phys. Rev. Lett. **99**, 178103 (2007).

[23] Y. Fily and M. C. Marchetti, Phys. Rev. Lett. **108**, 235702 (2012).

[24] B. ten Hagen, S. van Teeffelen, and H. Löwen, J. Phys.: Condens. Matter **23**, 194119 (2011).

[25] H. Brenner and D. A. Edwards, *Macrotransport Processes* (Butterworth-Heinemann, New York, 1993).

[26] P. Hänggi, F. Marchesoni, S. Savelev, and G. Schmid, Phys. Rev. E **82**, 041121 (2010).

[27] F. Marchesoni and S. Savelev, Phys. Rev. E **80**, 011120 (2009).

[28] F. Marchesoni, J. Chem. Phys. **132**, 166101 (2010).

[29] M. Borromeo and F. Marchesoni, Chem. Phys. **375**, 536 (2010).

[30] P. S. Burada, P. Hänggi, F. Marchesoni, G. Schmid, and P. Talkner, Chem. Phys. Chem. **10**, 45 (2009).

[31] S. van Teeffelen and H. Löwen, Phys. Rev. E **78**, 020101(R) (2008).

[32] P. Dhar, Th. M. Fisher, Y, Wang, T. E. Mallouk, W. F. Paxton, and A. Sen, Nano Lett. **6**, 66 (2006).

[33] M. Ripoll, P. Holmqvist, R. G. Winkler, G. Gompper, J. K. G. Dhont, and M. P. Lettinga, Phys. Rev. Lett. **101**, 168302 (2008).

[34] I. Buttinoni, J. Bialkè, F. Kümmel, H. Löwen, C. Bechinger, and T. Speck, Phys. Rev. Lett. **110**, 238301 (2013).

[35] D. Takagi, J. Palacci, A. B. Braunschweig, M. J. Shelley, and J. Zhang, Soft Matter **10**, 1784 (2014).

[36] Y. Ai and S. Qian, Phys. Chem. Chem. Phys. **13**, 4060 (2011).